Chemical Engineering Journal 379 (2020) 122285

Contents lists available at ScienceDirect

Chemical Engineering Journal

journal homepage: www.elsevier.com/locate/cej

Laser-induced plasmonic heating in copper nanowire fabric as a photothermal catalytic reactor

Cheng-Chieh Chuang[a,1], Hsun-Chen Chu[a,1], Sheng-Bor Huang[a], Wei-Shun Chang[b,*], Hsing-Yu Tuan[a,*]

[a] Department of Chemical Engineering, National Tsing Hua University, 101, Section 2, Kuang-Fu Road, Hsinchu, Taiwan 30013, China
[b] Department of Chemistry and Biochemistry, University of Massachusetts Dartmouth, 285 Old Westport Rd, North Dartmouth, MA 02747, United States

HIGHLIGHTS

- A facile method to fabricate a robust Cu nanostructure at cm^2 is demonstrated.
- The CuNW fabric exhibits > 40% absorptance at 500–1200 nm.
- The CuNW fabric maintains a constant temperature at 250 °C under laser illumination.
- The photon-illuminated CuNW fabric leads to a rapid CuAAC reaction with more than 90% yield.

GRAPHICAL ABSTRACT

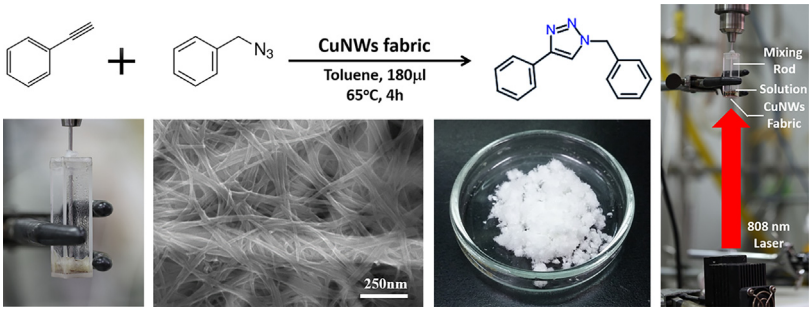

ARTICLE INFO

Keywords:
Copper nanowire
Photothermal conversion
Catalytic reactor
Plasmonics

ABSTRACT

Metallic nanostructures possessing higher surface-to-volume ratio provide a more accessible surface to catalyze chemical reactions compared to the bulk materials. However, scaling up the nanostructures remains complicated and limits the applications as industrial catalysis. Here, we demonstrate a facile method to fabricate a robust and versatile Cu nanostructure at a centimeter scale as an efficient photothermal catalytic reactor. By drop-casting the solution of Cu nanowires into a Teflon mold after solvent evaporation followed by annealing in the H_2/Ar atmosphere, a Cu nanowire fabric possessing a network structure with a high density of porosity is formed. The Cu fabric exhibits a strong absorptance at the spectral range of 400–1200 nm owing to the interband transition, the surface plasmon resonances of Cu nanowires with their near-field coupling, and "light trapped effect" in the network structures. Exposure to 808 nm laser allows for the elevation of the temperature across the whole structure within 2 s and maintaining a stable temperature up to 250 °C for 2 h. A heterogeneous copper-catalyzed azide-alkyne cycloaddition reaction is performed using Cu nanowire fabric illuminated by an 808 nm laser. A repeatable yield of > 90% with a reaction time of 4 h, an order of magnitude shorter than conventional copper catalysts at ambient temperature, is achieved suggesting the Cu nanowire fabric as a robust photothermal catalytic reactor.

* Corresponding authors.
E-mail addresses: wchang2@umassd.edu (W.-S. Chang), hytuan@che.nthu.edu.tw (H.-Y. Tuan).
[1] These authors contributed equally to this work.

https://doi.org/10.1016/j.cej.2019.122285
Received 30 January 2019; Received in revised form 18 June 2019; Accepted 17 July 2019
Available online 18 July 2019
1385-8947/ © 2019 Elsevier B.V. All rights reserved.

1. Introduction

Surface plasmon resonances of metallic nanostructures have attracted significant attention in the past decades for the applications of catalysis [1–5], sensing [6–8], solar cell [9–11], biomedical treatment [12–14], and nano-optics [15–17]. In addition to the wavelength tunability by changing the size, shape, and surrounding environment [17,18], plasmonic nanoparticles also possess huge absorption cross section owing to strong light-matter interactions [19]. Because of negligible radiative relaxation, i.e., photoluminescence quantum yield of $< 10^{-6}$ [20,21], the absorbed photons relax nonradiatively into heat very efficiently and induce high temperature around nanoparticle followed by the heat dissipation to the surroundings [22]. This efficient photothermal conversion enables generating nanoscaled heat source using photoexcitation and benefits in several applications. For example, gold nanorods [23] or nanoshells [24] are functionalized with an antibody to attach to cancer or tumor cells selectively. By illuminating with a Near-IR laser at the biologically transparent window, the high temperature around the nanostructures induced by the absorbed photons further kills cancer and tumors cells. Gold nanoparticles are also used to distill organic solvents [25] and generate steam [26,27] for sterilization when irradiated by sunlight. Furthermore, the local heat near the nanoparticles also thermally enhances the chemical processes, and therefore higher reaction yield is obtained [28–30].

While Au and Ag nanostructures have been well studied for the thermoplasmonics [31], Cu, another element in the group 11 of the periodic table, has received less attention. Cu, compared to Au and Ag, has larger electron conductivity and higher earth abundance. These properties make Cu attractive as a low-cost plasmonic material. In addition to the earth abundance, Cu nanostructures also possess several advantages compared to their Au and Ag counterparts. Because of CMOS compatibility and excellent electric conductivity, Cu is widely used for the interconnection in integrated circuit. Cu and Cu oxide are catalysts for many chemical reactions including coupling reaction [32], detoxification reaction [33], and water-gas shifts [34]. They are also one of the best electro- and photo-catalysts for CO_2 reduction reaction [35–37] to convert harmful greenhouse gas into valuable fuel molecules, e.g., multi-carbon alcohols, alkenes, and aldehydes. The nanosized structures also possess a higher surface-to-volume ratio compared to the bulk metal providing more accessible surface during the reaction. Despite these excellent properties of the Cu nanostructures, bulk fabrication of the Cu nanoparticles through chemical synthesis is relatively problematic because it is more challenging to reduce Cu^{II} or Cu^{I} into Cu^{0} in aqueous solution. This obstacle hinders the control of the nanoparticles' facets which are essential for the selectivity and reactivity of metal catalysts.

Various Cu nanoparticles were synthesized [38–40] to catalyze CO_2 reduction [35,40], hydrogenation [41], and propylene epoxidation [42]. In addition to wide range of accessible oxidation states (Cu^{III}, Cu^{II}, Cu^{I}, and Cu^{0}) to promote the chemical reactions, the excitation of surface plasmon resonances of the Cu nanostructures further improves the activity and selectivity during the catalysis [41,42]. These enhancements arise from the decay of plasmon generating either energetic electrons or heat on the surface of nanostructures to catalyze chemical reactions. The yield of the energetic electrons and heat is scaled with the absorption cross section of the nanostructures. Despite the high absorption cross section, the plasmonic structures also scatter photons more efficiently if the size of the nanoparticle is larger than 100 nm [19]. This efficient scattering competes with the absorption and reduces the absorption efficiency of the nanoparticles. Therefore, engineering the structures of Cu nanoparticle assemblies is desired to enhance the harvest of photons. Additionally, it is also necessary to develop a facile method to assemble Cu nanoparticles onto an extensive area to scale up the catalytic reactions in the industry.

Herein, we developed a robust and versatile Cu nanowire (CuNW) fabric in cm^2 scale by simply drop-casting CuNW solution into a mold. A strong absorbance at wide spectral range of 400–1200 nm was achieved arising from interband transition, the near-field coupling of surface plasmon resonances, and light-trapping in the interior of fabrics. Excitation by an 808 nm laser with a beam size of 0.16 cm^2 induced the temperature of the CuNW fabric to homogeneously rise to 250 °C within 2 s and the temperature remained constant for more than 2 h without a noticeable structural change. Using CuNW fabric illuminated by an 808 nm laser as a thermal catalytic reactor, a heterogeneous copper-catalyzed azide-alkyne cycloaddition (CuAAC) reaction was performed exhibiting a repeatable product yield of 97% and reaction time of 4 h, an order of magnitude shorter than the conventional method. These results suggest CuNW fabric as a robust and large-scaled photothermal catalytic reactor.

2. Experimental Section

2.1. Materials

Dichloromethane (CH_2Cl_2, ≧99.8%), chloroform-d ($CDCl_3$, 99.8 atom % D), oleylamine (OLA, $C_{18}H_{37}N$, 70%), and toluene ($C_6H_5CH_3$, 99.9%) were purchased from Sigma-Aldrich. Copper chloride (CuCl, 99.99%), phenyl acetylene (C_6H_5CCH, 98 + %), benzyl azide ($C_6H_5CH_2N_3$, 94%), ethyl acetate ($CH_3COOCH_2CH_3$, ACS grade) were purchased from Alfa, and hexane (ACS grade) was purchased from Marcon. Silica gel (SiOH) disposable extraction columns and acetone ($(CH_3)_2CO$, ACS) were purchased from J.T Baker. Cu foil was purchased from Shining Energy Co., Ltd. All materials were used without further purification.

2.2. Synthesis of the Cu nanowires

OLA-capped copper nanowires (CuNWs) were synthesized based on the method developed by the previous work [43,44] with some modifications. Essentially, 3 mmol of CuCl was added into a 50 ml three-neck flask sealed with a rubber stopper in a glovebox. After the flask was removed from the glovebox, 30 ml of OLA was injected into the flask that was subsequently connected to a Schlenk line and purged with argon. The solution in the flask was heated to 110 °C for 50 min and magnetically stirred under an inert atmosphere. During this process, the color of the solution changed from green to clear yellow. The solution was then heated and maintained at 250 °C for 50 min, and the color of the solution changed to reddish brown. After cooling to room temperature, the solution was dispersed in hexane and centrifuged at 8000 rpm for 7 times until the upper suspension became completely clear. The precipitation (CuNWs) was stored in the glovebox.

2.3. Preparation of CuNW fabric

5 mg of OLA-capped CuNWs were dispersed in toluene (500 μl), and the solution was dropped into a square Teflon mold. The mold was heated to 60 °C on a hot plate, and the CuNW fabric was obtained after evaporating the toluene. After removing from the mold, the CuNW fabric was placed in a furnace under an atmosphere composed of 5% H_2 and 95% Ar and was annealed at 360 °C for 3 h to remove OLA on the NW surface and to reduce the copper oxide. Subsequently, the CuNW fabric was stored in the glovebox. The procedures of fabricating the CuNW fabric are illustrated in Fig. S1.

2.4. Measurement of the temperature rise due to photothermal effects

The CuNW fabric was placed on a square holder inside a vacuum chamber with two glass windows as schematically illustrated in Fig. S2a. The pressure of chamber was kept at 10^{-1} torr during the measurement. The photograph of CuNW fabric in the vacuum chamber is shown in Fig. S2b. An 808 nm laser (Civil Laser, 808 nm 2 W) was employed to illuminate on the surface of CuNW fabric, and the

temperature of the CuNW fabric was measured by a fiber optic thermometer (Japan Sensor Corporation, FTK9-R160A-10S21). The photograph of the apparatus is displayed in Fig. S2c. The temperature of CuNW fabric was adjusted accordingly by the laser power.

2.5. Synthesis of 1-benzyl-4-phenyl-1H-1,2,3-triazole via huisgen 1,3-dipolar cycloaddition catalyzed by the CuNW fabric

A 1 cm × 1 cm sample of CuNW fabric, 180 μl of toluene, 112 μl of phenyl acetylene (1 mmol) and 133 μl of benzyl azide (1 mmol) were added in a quartz cuvette. After sealing the cuvette, the solution was stirred using a steel rod followed by illumination with the 808 nm laser. The temperature of the solution was held at 65 °C for 4 h by adjusting the laser power at 1500 mW. The temperature was measured by a thermocouple attached to the quartz cuvette. After cooling to room temperature, white precipitation appeared in the solution. Subsequently, 2.5 ml dichloromethane was added into the cuvette to dissolve the product and the CuNW fabric was removed from the solution. The solution was injected through a syringe filter to remove residual CuNWs, and the solvent of the filtered solution was then removed using a rotary evaporator. The residual white powder was further purified via column chromatography (silica gel) using hexane and ethyl acetate (3: 1, v/v) to obtain the final product of 1-benzyl-4-phenyl-1H-1,2,3-triazole verified by nuclear magnetic resonance (NMR) spectroscopy (Fig. S3).

2.6. Characterization

TEM was performed using a Hitachi H-7100 electron microscope with an accelerating voltage of 75 kV. High-resolution TEM (HRTEM) images were obtained using a JEOL JEM 3000F electron microscope with an accelerating voltage of 200 kV. SEM was performed using a Hitachi SU8080 field emission scanning electron microscope. XRD measurements were carried out by a MAC Science MXP18 diffractometer with CuKa radiation. The X-ray photoelectron spectroscopy (XPS) was obtained using a ULVAC-PHI AES650 high-resolution X-ray photoelectron spectrometer (HR-XPS). The NMR spectra were measured by a Varian UNIYTINOV 500 NMR spectrometer.

3. Results and Discussions:

The CuNWs were synthesized by reacting $CuCl_2$ with OLA based on the previous publication [43,44]. The diameter and length of CuNWs are ~ 55 nm and 5 to tens of μm, respectively. (Fig. S4a and b) The single crystallinity of the CuNWs was confirmed by XRD (Fig. S4c) which showed three apparent peaks at 2θ = 43.316°, 50.448° and 74.125° corresponding to (1 1 1), (2 0 0) and (2 2 0) planes, respectively, in agreement with the face-centered-cubic of Cu (JCPDS No. 89–2838). The CuNW fabric was fabricated by drop casting the CuNW solution into a Teflon mold followed by annealing in a furnace. (See experimental section for the details) Fig. 1a shows the top view of the SEM image of a CuNW fabric. The high density of CuNWs forms a random network structure with very high porosity that allows molecules to diffuse freely in the interior of fabric. The SEM image of the cross section of CuNW fabric (Fig. 1b) displays the porous network structure with a thickness of ~22 μm. Interestingly the dark brown color of CuNW in the photograph (Inset of Fig. 1a) suggests less reflection due to the rough surface of the fabric. Further, a Cu foil with an area of 1 × 1 cm^2 was also employed to investigate the morphology dependence of the absorption and the photothermal conversion that will be discussed later. Compared to the CuNW fabric, the SEM image of the Cu foil (Fig. 1c) shows a much smoother surface that induces higher reflection of the incident light. This is evidenced by the shiny metal color in the photograph of the Cu foil displayed in the inset of Fig. 1c. As expected, the cross section of the Cu foil indicates a solid metal film with a thickness of 10.5 μm. (Fig. 1d)

CuNW fabric shows a higher absorptance than Cu foil. In order to quantify the absorptance of CuNW fabric and Cu foil, we measured the transmittance and reflectance spectra of these samples using a UV-VIS-NIR spectrometer equipped with an integrating sphere. The absorptance was calculated by $A = 1 - T - R$, where A, T, and R are absorptance, trasmittance and reflectance, respectively. The transmittance spectra of the CuNW fabric and Cu foil were obtained by placing the sample on the entrance port of the integrating sphere, where all the transmission photons were collected [45]. The total reflectance was measured when the samples located at the reflectance port at the back of the integrating sphere. As a result, all the photons reflected by the fabric or foil were detected. Fig. 2a shows the transmittance of CuNW fabric (red) and Cu foil (black) with ~0% independence of the wavelengths while the reflectance spectra of these two samples are substantially different (Fig. 2b). For the Cu foil, a low refelctance (30–50%) was observed with a wavelength shorter than 600 nm, which was the onset of the interband transition of Cu [46]. A very high reflectance (> 90%) was detected at the spectral range of 600–1200 nm leading to the shiny metal color of Cu foil as shown in the photograph. (Inset of Fig. 1c) Contrarily, the reflectance of CuNW fabric was ~15% above the interband transition of Cu and 40–60% at 600–1200 nm. The much lower reflectance in the CuNW fabric compared to Cu foil arose from two mechchnisms: (1) a rough surface to reduce the diffusion and specular reflectance; (2) the network structure where the photons incident into the interior of the fabric underwent multiple reflection and eventually were absorbed by CuNWs. As a result, the absorptance of CuNW fabric (red) was higher than that of Cu foil (black) depicted in Fig. 2c for all wavelengths. The absorptance spectrum of Cu foil showed a very low absorptance (< 10%) at spectral range of 600–1200 nm and an interband transition of Cu (50–70%) at wavelengths shorter than 600 nm. For CuNW fabric, a strong absorptance of > 40% at 600–1200 nm and ~85% above interband transition was observed.

The large absorbance of the CuNW fabric at 600-1200 nm arises from the surface plasmon of the CuNWs and possibly their near-field coupling at the junction between the NWs. The extinction spectrum of single CuNW was calculated using the boundary element method [47] with the diameter and length of 55 nm and 5 μm, respectively, as discussed in Fig. S5. Several higher order longitudinal modes were observed at the range of 600–1200 nm. It is also expected that the peaks of the higher order modes would be located at different wavelengths for various lengths of NWs because the energies of the higher order modes depend on the aspect ratio (length/diameter) of NWs. Therefore, the length heterogeneity of the NWs caused a very broad absorption spectrum at 600–1200 nm. Additionally, it is well established that the surface plasmons strongly couple when two nanostructures are in closed proximity [48]. The network structures of CuNW fabric possessing a high density of junctions could lead to the near-field coupling between the plasmon modes. These hybrid plasmon modes induced more abundant plasmon modes [49,50] which redshifted or blueshifted compared to the uncoupled modes depending on the coupling geometry and polarization of incident light [51]. The coupled plasmonic modes also enhanced the absorption cross section [52–54]. As a result, the absorption spectrum was further broadened and amplified. More importantly, the network structure of the fabric induced “light trap”. When the photons were incident into the interior of fabric, they were scattered by NWs multiple times inside the network, and finally absorbed by the NWs either via interband transition or surface plasmon resonances. Thereby, the stronger absorption at the range of 400–1200 nm was achieved as shown in Fig. 2c.

Due to higher absorptance, the CuNW fabric demonstrated an efficient photothermal conversion to generate more heat compared to Cu foil. In order to quantify the photothermal conversion on the nanostructures, we measured the temperature of CuNW fabric and Cu foil, respectively, under the illumination of an 808 nm laser in vacuum. (see the experimental section for the details) The 808 nm laser was chosen because it can excite surface plasmon resonance of CuNW. It is also

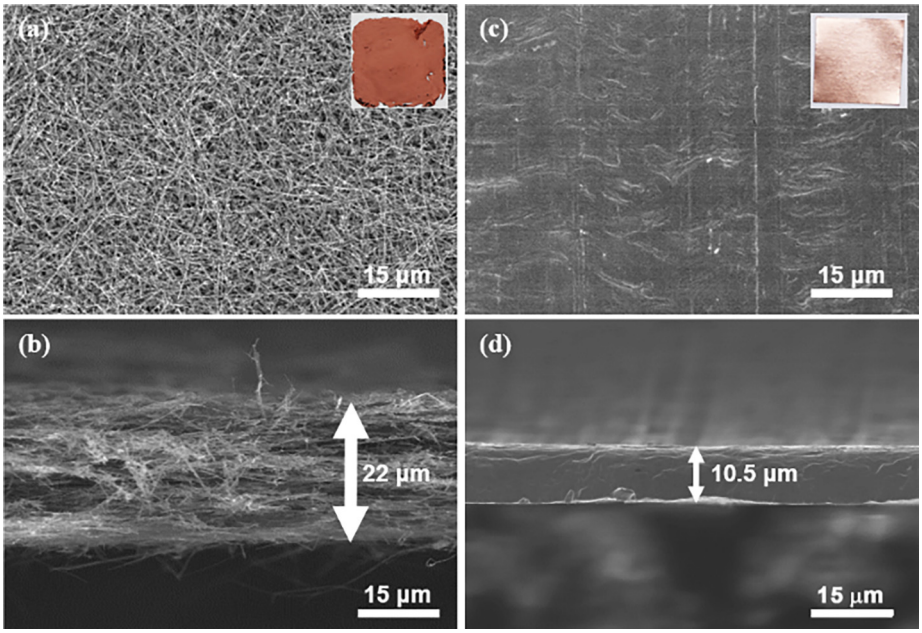

Fig. 1. SEM images of CuNW fabric and Cu foil. (a) Top view, (b) side view of CuNW fabrics. (c) Top view, (d) side view of Cu foil. The insets of (a) and (c) are the photographs of CuNW fabric and Cu foil, respectively, with sizes of 1 × 1 cm^2. The thickness of CuNW fabric and Cu foil are 22 and 10.5 μm, respectively.

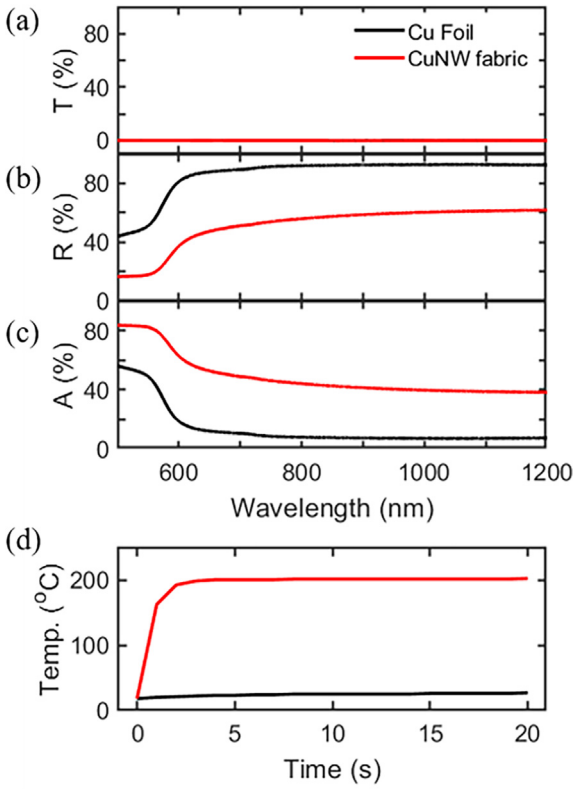

Fig. 2. The spectra of Cu foil and CuNW fabric. (a) Transmission, (b) reflectance, and (c) absorptance of Cu foil (black) and CuNW fabric (red). (d) The temperature of Cu foil (black) and CuNW fabric (red) as a function of exposure time to an 808 nm laser.

cost-effective making it a potential candidate for industrial application. The beam size was estimated as ~0.16 cm^2 and was much smaller than the sample size of 1 cm^2. After laser irradiation, the temperature increased in the whole CuNW fabric according to the image recorded by a IR camera (Fig. S6). The temperature on the samples was probed by a fiber optic thermometer at the identical area under laser exposure. Probing the temperature under vacuum allowed minimizing the heat loss to the environment and enhancing more uniform heating on the whole fabric or foil in a shorter time. Fig. 2d shows the temperature of CuNW fabric (red) and Cu foil (black) as a function of exposure time under the continuous illumination of an 808 nm laser. With an excitation power of 937 mW, the temperature of CuNW fabric increased to 200 °C within 2 s and then maintained at 200 °C, while there was almost no rise in temperature for the Cu foil. The large and fast temperature rise followed by the steady temperature showed the superiority of the CuNW fabric that efficiently converted photon energy into heat and reached thermal equilibrium rapidly. More importantly, the temperature elevated in the whole CuNW fabric even with a smaller illuminated area due to the high density of junctions in the network structure. When the photons were absorbed by the CuNWs, most of the absorbed energy relaxed nonradiatively into heat and transferred to the lattice of the wires followed by a fast heat diffusion inside the wires. The junctions between the wires also facilitated heat transport to the other wires that were not photoexcited. Furthermore, the photons inside the network were scattered multiple times and absorbed by the CuNWs outside the initial illumination area. Therefore, the temperature of the whole fabric of 1 cm^2 can rise within 2 s under an illumination area of 0.16 cm^2. Such efficient photothermal conversion in a large area (cm^2) suggests that the Cu NW fabric is a good candidate as a thermal reactor to catalyze the chemical reactions on a large scale. An excellent thermal reactor should maintain a constant temperature during the reaction. Next, we investigated the stability of the temperature at different laser power.

The constant temperature of CuNW fabric can be achieved up to 250 °C with continuous exposure to an 808 nm laser. To test the structural stability under the IR radiation, we have measured the temperature of the CuNW fabric at various laser power. Shown in Fig. 3a, the temperature rose and reached the steady state within the first 2 s and then remained constant under the continuous illumination of the 808 nm laser with the power at less than 1087 mW. At 1087 mW, the steady-state temperature reached 250 °C. The temperature increased with the laser power. We also observed a fluctuation in the temperature of the CuNW fabric after 2 s when the laser power was higher than 1162 mW. (purple and red lines in Fig. 3a). These temperature fluctuations were possibly due to the melting of the NWs during the laser illumination leading to the change of the absorption of the CuNW

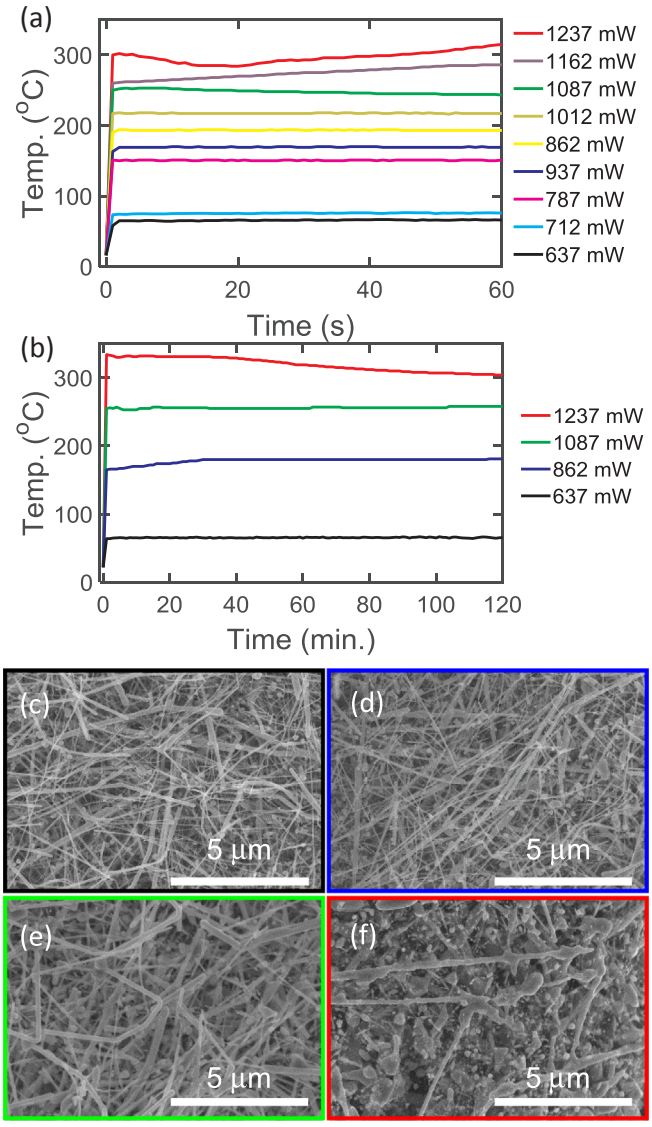

Fig. 3. The temperature trace and SEM images of CuNW fabric radiated by an 808 nm laser at various power. (a) The temperature of CuNW fabric as a function of exposure time with a period of 1 min at various laser power. (b) The temperature of CuNW fabric as a function of exposure time with a period of 2 h at 637 (black), 862 (blue), 1087 (green), and 1237 mW (red). SEM images of CuNW fabric after illuminated by an 808 nm laser for 2 h at power of (c) 637 mW, (d) 862 mW, (e) 1087 mW, and (f) 1237 mW. The colored frames of SEM images corresponding to the line colors of temperature traces are shown for reference.

fabric.

The temperature instability was caused by the melting of the CuNW fabric when illuminating with a laser power higher than 1087 mW. To test the stability of the CuNW fabric, we measured the temperature of CuNW fabric under continuous exposure for 120 min at varying power. Four representative powers were chosen to demonstrate the stability of the CuNW fabric for a longer period of time. The temperature kept constant after an initial rise with the laser power at less than 1087 mW (black, blue, and green lines in Fig. 3b) and decreased with time when the laser power was 1237 mW (red line in Fig. 3b). To understand the cause of the temperature instability, we utilized SEM to characterize the morphology of the CuNW fabric after illumination by an 808 nm laser for 2 h. Fig. 3c–f depict the SEM images of CuNW fabric after exposure to the laser at a power of 637, 862, 1087, and 1237 mW, respectively. The CuNW fabric still maintained the network structure with the power less than or equal to 1087 mW (Fig. 3c–e) suggesting no melting of the NWs. However, the CuNWs disappeared and fused into a large chunk of irregular structures in the fabric at a laser power of 1238 mW (Fig. 3f). The fused structures in Fig. 3f suggested the melted CuNWs with high laser power observed in other studies [55]. When the NWs were melted, the longitudinal surface plasmon resonance disappeared leading to the reduction of absorption at 808 nm. Therefore, the temperature rise was lower when illuminating at the same power. This explained the decrease of the temperature with time shown in the red curve of Fig. 3b. We concluded that the CuNW fabric can sustain temperatures up to 250 °C under the exposure of an 808 nm laser. It is noted that the transient temperature on CuNW fabric under laser illumination could be much higher than the equilibrium temperature that is probed by the fiber optics thermometer. This high transient temperature originates from the fact that absorbed energy relaxes into hot electrons and then transfers to the lattice of CuNWs before reaching the thermal equilibrium with environment. The transient temperature on CuNWs is higher than 350 °C at an excitation power of 1237 mW because we did not observe the melting of CuNWs at 350 °C during thermal annealing.

Further, we utilized CuNW fabric as a catalyst to drive a chemical reaction. Cu based nanostructures are widely used to catalyze chemical reactions [56–58]. To show the efficient photothermal conversion of CuNW fabric for the Cu based catalysis, we performed a heterogeneous copper-catalyzed azide-alkyne cycloaddition (CuAAC) click reaction with the reaction equation shown in Fig. 4a. The CuAAC reaction has been utilized to make covalent bond between building blocks with various functions [59,60]. This reaction produces products with high yields and a fast rate at ambient temperature and thus is used for organic synthesis, bioconjugation, medicine chemistry, and polymer chemistry. Conventionally, the catalyst for this reaction is the Cu^{I} ion sourced from the Cu^{I} salt or coordination complexes [60]. The Cu^{I} ions act on the terminal alkyne to generate Cu^{I} acetylides that immediately react with the organic azides to form triazole compounds [61]. However, the Cu^{I} ions might induce the copper contamination in the products [62]. As a result, the element Cu (Cu metal) [63] was introduced in the CuAAC reaction to yield high purity of triazole products with minimum copper contamination despite requiring a long reaction time (12–48 h) at ambient temperature [63–65].

The CuNW fabric under 808 nm laser excitation during CuAAC reaction produces triazole compounds with 97% yield within 4 h. We synthesized 1-benzyl-4-phenyl-1H-1,2,3-triazole via CuAAC reaction using phenyl acetylene and benzyl azide as reactants. (See Experimental Section for the details) After adding phenyl acetylene, benzyl azide, toluene, and CuNW fabric into a sealed quartz cuvette, the reactants were thoroughly mixed by a stirring rod (Fig. 4b), and the solution was transparent with a light yellow color (Fig. 4c). The temperature was maintained at 65 °C for 4 h by illuminating 808 nm laser on the cuvette. The solution was cooled down gradually to room temperature after turning off the laser. During the cooling process, white solids appeared in the solution as depicted in Fig. 4d. After purification by column chromatography, we obtained a white powder (Fig. 4e), 1-benzyl-4-phenyl-1H-1,2,3-triazole, as verified by NMR spectroscopy (Fig. S3). The white powder was massed at 228.0 mg which corresponded to 0.97 mmol and a product yield of 97%. The high yield with fast reaction time (~4 h) originated from the higher reaction temperature [63,65] caused by the efficient photothermal conversion of CuNW fabric. A control experiment without laser illumination was performed and resulted in a negligible yield of 1-benzyl-4-phenyl-1H-1,2,3-triazole. Since the temperature remained constant at 65 °C during the CuAAC reaction, we expect no melting of the CuNW during the reaction.

The CuAAC intermediates utilization of the CuNW fabric was consistent with Cu^{I} salts forming Cu^{I} acetylides after reacting with alkynes [61] used to initiate the reaction. To verify the mechanism, we characterized the CuNW fabric by SEM images and XPS spectra in three steps: (1) pristine CuNW fabric, (2) after only adding phenyl acetylene, (3) after completing the CuAAC reaction. Before the reaction, the SEM

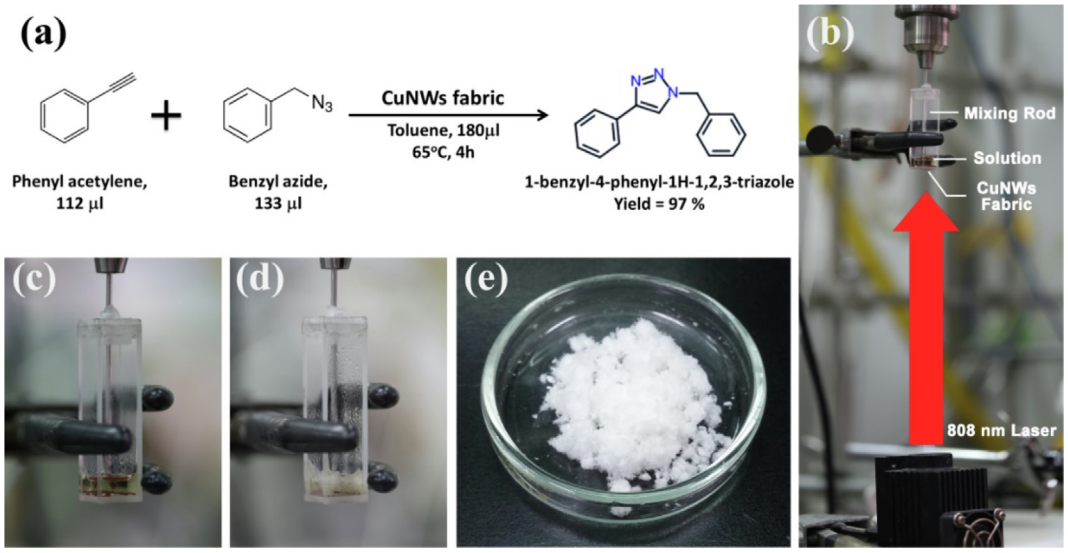

Fig. 4. (a) The chemical equation of CuAAC reaction. Phenyl acetylene and benzyl azide in toluene were catalyzed by CuNW fabric at 65 °C induced by laser excitation and produced 1-benzyl-4-phenyl-1*H*-1,2,3-triazole. (b) The photograph of the apparatus for the CuAAC reaction. The reactants were placed in a cuvette and thoroughly mixed by a stirring rod. An 808 nm laser illuminating on the bottom of the cuvette induced the temperature rise on CuNW fabric. (c) The photograph of the solution, which appeared light yellow, before laser irradiation. (d) The photograph of the solution after illuminated by the laser for 4 h. The solution became white solid. (e) The photograph of the final product identified as 1-benzyl-4-phenyl-1*H*-1, 2, 3-triazole by NMR spectroscopy.

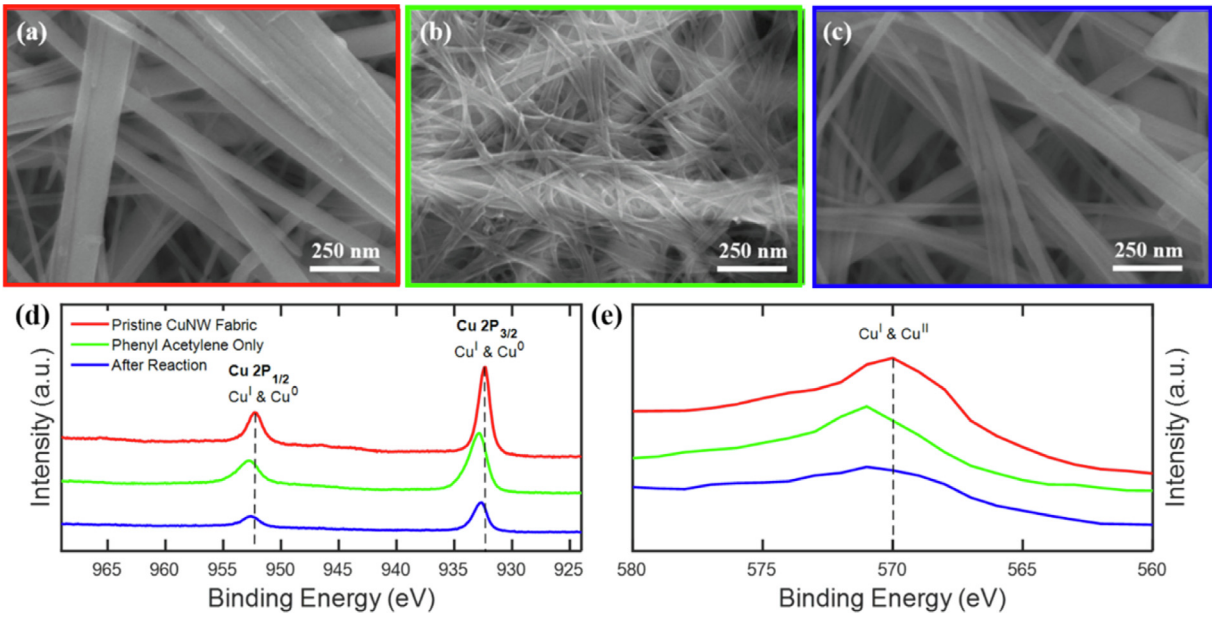

Fig. 5. SEM images and XPS spectra of CuNW fabric during CuAAC reaction. SEM image of (a) the pristine CuNW fabric, (b) the CuNW fabric after adding phenyl acetylene, and (c) the CuNW fabric after completing CuAAC reaction. (d-e) XPS spectra of the pristine CuNW fabric (red), the CuNW fabric after adding phenyl acetylene (green), and the CuNW fabric after reaction (blue) in the Cu 2p (d) and the Cu LMM (e) regions. The vertical dashed lines are the guides to the eyes. The colored frames of SEM images corresponding to the line colors of XPS spectra are shown for reference.

image of the CuNW fabric showed a clean surface of the NWs in the network structures (Fig. 5a). After adding the phenyl acetylene to the CuNW fabric, the surface of the CuNW fabric was covered with a dielectric layer and showed less contrast in the SEM image (Fig. 5b). This dielectric layer could be Cu^{I} acetylides, as supported by the previous study[61]. Additionally, the network structure of the CuNW fabric allowed phenyl acetylene diffusing into the interior of the CuNW fabric to form a thin layer of Cu^{I} acetylides for further reaction. After adding benzyl azide and exposing to an 808 nm laser for 4 h, the dielectric layer was almost diminished from the surface of the CuNW as shown in Fig. 5c. This result suggested that the Cu^{I} acetylides reacted with benzyl azide to yield 1-benzyl-4-phenyl-1H-1,2,3-triazole. It is noted that the NW surface was not as smooth as the pristine CuNW fabric possibly arising from the residue of Cu(I) acetylides or atom migration during the reaction. The result of the XPS spectra also supported the observation in the SEM. The red, green, and blue lines in Fig. 5d, e correspond to the XPS spectra of the pristine CuNW fabrics, the CuNW fabric after adding phenyl acetylene, and the CuNW fabric after the CuAAC reaction, respectively. The XPS spectra of the pristine CuNW fabric in Fig. 5d shows two strong peaks at 932 and 952 eV with several low-intensity bumps at 935, 945, 954, and 964 eV. The Cu $2P_{2/3}$ and $2P_{1/2}$ located at 932 and 952 eV, respectively, originated from Cu^{0} and Cu^{I} while the small bumps were attributed to the Cu^{II}. As the detection depth of the XPS is ~ 5 nm, the signal of Cu^{I} suggests a formation of

Cu_2O on Cu after the CuNW fabric exposing to air. After adding phenyl acetylene to CuNW fabric, the Cu $2P_{2/3}$ and $2P_{1/2}$ peaks of Cu^0 and Cu^I (green line in Fig. 5d) blueshifted and broadened compared to those of the pristine CuNW fabric (red line in Fig. 5d). The broader and higher energy peak possibly arose from the formation of Cu^I acetylides after Cu^I reacted with phenyl acetylene. The Cu^I ion possibly originated from Cu_2O or from the partial reaction of Cu^0 and Cu^{II} [59,65,66]. The Cu $2P_{2/3}$ and $2P_{1/2}$ peaks of Cu^0 and Cu^I (blue line in Fig. 5d) red-shifted and narrowed when the CuAAC reaction was completed suggesting the elimination of the Cu^I acetylides on the surface of CuNWs. These observations were consistent with the proposed mechanism of CuAAC reaction in the presence of Cu^I [59,61]. Therefore, we attributed the change of the position and linewidth of Cu $2P_{2/3}$ and $2P_{1/2}$ peaks to the participation of Cu^I in the CuAAC reaction. We also noticed that the Cu $2P_{2/3}$ and $2P_{1/2}$ peaks of Cu^I after the CuAAC reaction (blue line) were still slightly blueshifted compared to those of the pristine CuNW fabric (red line). This result indicated that the residue of the Cu^I acetylides was consistent with the observation from SEM. The participation of the Cu^I in CuAAC reaction was further confirmed by analysis of Cu LMM peaks for the CuNW fabric shown in Fig. 5e. The peak at 570 eV in the pristine CuNW fabric (red line) corresponds to the Cu LLM peak of Cu^I. The Cu LMM peak shifted to a higher energy (green line) after adding phenyl acetylene to the CuNW fabric. Similar to the Cu 2P peaks, the Cu LLM peak redshifted after the CuAAC reaction (blue line), with the peak energy slightly higher than that of the pristine CuNW fabric. This result was again consistent with the residue of Cu^I acetylides on Cu NW surface after the CuAAC reaction. Despite the organic residues on the metal surface after the reaction, the CuNW fabric was very stable for the CuACC reactions. To test the reusability of the CuNW fabric, we have utilized the same CuNW fabric to repeat the CuAAC reaction 5 times. The yield of 1-benzyl-4-phenyl-1H-1,2,3-triazole was higher than 90% for each reaction (Fig. S7). This result indicates that CuNW fabric is a stable catalyst for the CuAAC reaction. It is also worth noting that the conventional catalysts such as Cu^I salts or coordination complexes for the CuAAC reaction require an additional separation process in order to recycle the catalysts. Such separation process is not needed for the CuNW fabric because it can be reused after washing away the products. Therefore, the CuNW fabric can further simplify the processes of recycling catalysts for the CuAAC reaction.

4. Conclusion:

In summary, we demonstrate a new concept for a remotely controlled photothermal catalytic reactor based on a CuNW fabric. The CuNW fabric possesses strong absorbance at a broad range of 400–1200 nm arising from the interband transition, surface plasmon resonances with their near-field coupling, and light trapped in the network structure. Under illumination with an 808 nm laser, the robust CuNW fabric can achieve a constant temperature up to 250 °C within 2 s for more than 2 h. A demonstration of the CuAAC reaction using CuNW fabric under laser illumination produces triazole compounds with 97% yield and a rapid reaction rate. Repeating the CuAAC reaction 5 times using the same piece of CuNW fabric maintains a product yield of more than 90%. Such robust CuNW fabric is an ideal photothermal reactor to increase the reaction rate for Cu based catalytic reactions.

Acknowledgments

The authors acknowledge the financial support by the Ministry of Science and Technology through the grants of MOST 106-2221-E-007-081-MY3, 106-2628-E-007-005-MY3, 103-2221-E-007-089-MY3, and MOST 106-2622-8-007-017, and by National Tsing Hua University through the grant of 107Q2708E1. W.-S. C acknowledges the generous support through the startup fund from the University of Massachusetts Dartmouth and computational support from the Massachusetts Green High-Performance Computing Center. We thank Ms. Rachael Howland for help with editing the manuscript.

Appendix A. Supplementary data

Supplementary data to this article can be found online at https://doi.org/10.1016/j.cej.2019.122285.

References

[1] Y. Zhang, S. He, W. Guo, Y. Hu, J. Huang, J.R. Mulcahy, W.D. Wei, Surface-plasmon-driven hot electron photochemistry, Chem. Rev. 118 (2018) 2927–2954.
[2] M.L. Brongersma, N.J. Halas, P. Nordlander, Plasmon-induced hot carrier science and technology, Nat. Nano. 10 (2015) 25–34.
[3] U. Aslam, V.G. Rao, S. Chavez, S. Linic, Catalytic conversion of solar to chemical energy on plasmonic metal nanostructures, Nat. Catal. 1 (2018) 656–665.
[4] M.J. Kale, T. Avanesian, P. Christopher, Direct photocatalysis by plasmonic nanostructures, ACS Catal. 4 (2014) 116–128.
[5] J.B. Sambur, P. Chen, Approaches to single-nanoparticle catalysis, Annu. Rev. Phys. Chem. 65 (2014) 395–422.
[6] A.B. Taylor, P. Zijlstra, Single-molecule plasmon sensing: current status and future prospects, ACS Sens. 2 (2017) 1103–1122.
[7] B.S. Hoener, S.R. Kirchner, T.S. Heiderscheit, S.S.E. Collins, W.-S. Chang, S. Link, C.F. Landes, Plasmonic sensing and control of single-nanoparticle electrochemistry, Chem 4 (2018) 1560–1585.
[8] K.A. Willets, R.P.V. Duyne, Localized surface plasmon resonance spectroscopy and sensing, Annu. Rev. Phys. Chem. 58 (2007) 267–297.
[9] K. Ueno, T. Oshikiri, Q. Sun, X. Shi, H. Misawa, Solid-state plasmonic solar cells, Chem. Rev. 118 (2018) 2955–2993.
[10] H.A. Atwater, A. Polman, Plasmonics for improved photovoltaic devices, Nat. Mater. 9 (2010) 205.
[11] W.R. Erwin, H.F. Zarick, E.M. Talbert, R. Bardhan, Light trapping in mesoporous solar cells with plasmonic nanostructures, Energy Environ. Sci. 9 (2016) 1577–1601.
[12] O.S. Kolovskaya, T.N. Zamay, I.V. Belyanina, E. Karlova, I. Garanzha, A.S. Aleksandrovsky, A. Kirichenko, A.V. Dubynina, A.E. Sokolov, G.S. Zamay, Y.E. Glazyrin, S. Zamay, T. Ivanchenko, N. Chanchikova, N. Tokarev, N. Shepelevich, A. Ozerskaya, E. Badrin, K. Belugin, S. Belkin, V. Zabluda, A. Gargaun, M.V. Berezovski, A.S. Kichkailo, Aptamer-targeted plasmonic photothermal therapy of cancer, Mol. Ther. Nucleic Acids 9 (2017) 12–21.
[13] X. Huang, P.K. Jain, I.H. El-Sayed, M.A. El-Sayed, Plasmonic photothermal therapy (PPTT) using gold nanoparticles, Lasers Med. Sci. 23 (2007) 217.
[14] J.L. West, N.J. Halas, Engineered nanomaterials for biophotonics applications: improving sensing, imaging, and therapeutics, Annu. Rev. Biomed. Eng. 5 (2003) 285–292.
[15] M.L. Juan, M. Righini, R. Quidant, Plasmon nano-optical tweezers, Nat. Photonics 5 (2011) 349.
[16] N. Yu, F. Capasso, Flat optics with designer metasurfaces, Nat. Mater. 13 (2014) 139.
[17] A. Kristensen, J.K.W. Yang, S.I. Bozhevolnyi, S. Link, P. Nordlander, N.J. Halas, N.A. Mortensen, Plasmonic colour generation, Nat. Rev. Mater. 2 (2016) 16088.
[18] K.L. Kelly, E. Coronado, L.L. Zhao, G.C. Schatz, The optical properties of metal nanoparticles: the influence of size, shape, and dielectric environment, J. Phys. Chem. B 107 (2003) 668–677.
[19] M.A. van Dijk, A.L. Tchebotareva, M. Orrit, M. Lippitz, S. Berciaud, D. Lasne, L. Cognet, B. Lounis, Absorption and scattering microscopy of single metal nanoparticles, PCCP 8 (2006) 3486–3495.
[20] M. Yorulmaz, S. Khatua, P. Zijlstra, A. Gaiduk, M. Orrit, Luminescence quantum yield of single gold nanorods, Nano Lett. 12 (2012) 4385–4391.
[21] Y. Fang, W.-S. Chang, B. Willingham, P. Swanglap, S. Dominguez-Medina, S. Link, Plasmon emission quantum yield of single gold nanorods as a function of aspect ratio, ACS Nano 6 (2012) 7177–7184.
[22] M. Hu, G.V. Hartland, Heat dissipation for Au particles in aqueous solution: relaxation time versus size, J. Phys. Chem. B 106 (2002) 7029–7033.
[23] M.R.K. Ali, Y. Wu, Y. Tang, H. Xiao, K. Chen, T. Han, N. Fang, R. Wu, M.A. El-Sayed, Targeting cancer cell integrins using gold nanorods in photothermal therapy inhibits migration through affecting cytoskeletal proteins, Proc. Natl. Acad. Sci. U.S.A. 114 (2017) E5655–E5663.
[24] C. Ayala-Orozco, C. Urban, M.W. Knight, A.S. Urban, O. Neumann, S.W. Bishnoi, S. Mukherjee, A.M. Goodman, H. Charron, T. Mitchell, M. Shea, R. Roy, S. Nanda, R. Schiff, N.J. Halas, A. Joshi, Au Nanomatryoshkas as efficient near-infrared photothermal transducers for cancer treatment: benchmarking against nanoshells, ACS Nano 8 (2014) 6372–6381.
[25] O. Neumann, A.D. Neumann, E. Silva, C. Ayala-Orozco, S. Tian, P. Nordlander, N.J. Halas, Nanoparticle-mediated, light-induced phase separations, Nano Lett. 15 (2015) 7880–7885.
[26] P.D. Dongare, A. Alabastri, S. Pedersen, K.R. Zodrow, N.J. Hogan, O. Neumann, J. Wu, T. Wang, A. Deshmukh, M. Elimelech, Q. Li, P. Nordlander, N.J. Halas, Nanophotonics-enabled solar membrane distillation for off-grid water purification, Proc. Natl. Acad. Sci. U.S.A. (2017).
[27] O. Neumann, C. Feronti, A.D. Neumann, A. Dong, K. Schell, B. Lu, E. Kim, M. Quinn, S. Thompson, N. Grady, P. Nordlander, M. Oden, N.J. Halas, Compact solar autoclave based on steam generation using broadband light-harvesting nanoparticles, Proc. Natl. Acad. Sci. U.S.A. 110 (2013) 11677–11681.

[28] C. Vázquez-Vázquez, B. Vaz, V. Giannini, M. Pérez-Lorenzo, R.A. Alvarez-Puebla, M.A. Correa-Duarte, Nanoreactors for simultaneous remote thermal activation and optical monitoring of chemical reactions, J. Am. Chem. Soc. 135 (2013) 13616–13619.
[29] F. Wang, C. Li, H. Chen, R. Jiang, L.-D. Sun, Q. Li, J. Wang, J.C. Yu, C.-H. Yan, Plasmonic harvesting of light energy for Suzuki coupling reactions, J. Am. Chem. Soc. 135 (2013) 5588–5601.
[30] L. Cao, D.N. Barsic, A.R. Guichard, M.L. Brongersma, Plasmon-assisted local temperature control to pattern individual semiconductor nanowires and carbon nanotubes, Nano Lett. 7 (2007) 3523–3527.
[31] G. Baffou, R. Quidant, Thermo-plasmonics: using metallic nanostructures as nano-sources of heat, Laser Photon. Rev. 7 (2013) 171–187.
[32] S. Uk Son, I. Kyu Park, J. Park, T. Hyeon, Synthesis of Cu2O coated Cu nanoparticles and their successful applications to Ullmann-type amination coupling reactions of aryl chlorides, Chem. Commun. (2004) 778–779.
[33] S. Vukojević, O. Trapp, J.-D. Grunwaldt, C. Kiener, F. Schüth, Quasi-homogeneous methanol synthesis over highly active copper nanoparticles, Angew. Chem. Int. Ed. 44 (2005) 7978–7981.
[34] T. Salmi, R. Hakkarainen, Kinetic study of the low-temperature water-gas shift reaction over a Cu—ZnO catalyst, Appl. Catal. 49 (1989) 285–306.
[35] D. Kim, C.S. Kley, Y. Li, P. Yang, Copper nanoparticle ensembles for selective electroreduction of CO_2 to C_2–C_3 products, Proc. Natl. Acad. Sci. U.S.A. 114 (2017) 10560–10565.
[36] T. Cheng, H. Xiao, W.A. Goddard, Nature of the active sites for CO reduction on copper nanoparticles; suggestions for optimizing performance, J. Am. Chem. Soc. 139 (2017) 11642–11645.
[37] I. Shown, H.-C. Hsu, Y.-C. Chang, C.-H. Lin, P.K. Roy, A. Ganguly, C.-H. Wang, J.-K. Chang, C.-I. Wu, L.-C. Chen, K.-H. Chen, Highly efficient visible light photocatalytic reduction of CO2 to Hydrocarbon Fuels by Cu-Nanoparticle Decorated Graphene Oxide, Nano Lett. 14 (2014) 6097–6103.
[38] S.-C. Lu, M.-C. Hsiao, M. Yorulmaz, L.-Y. Wang, P.-Y. Yang, S. Link, W.-S. Chang, H.-Y. Tuan, Single-crystalline copper nano-octahedra, Chem. Mater. 27 (2015) 8185–8188.
[39] H.-J. Yang, S.-Y. He, H.-L. Chen, H.-Y. Tuan, Monodisperse copper nanocubes: synthesis, self-assembly, and large-area dense-packed films, Chem. Mater. 26 (2014) 1785–1793.
[40] D. Kim, J. Resasco, Y. Yu, A.M. Asiri, P. Yang, Synergistic geometric and electronic effects for electrochemical reduction of carbon dioxide using gold–copper bimetallic nanoparticles, Nat. Comm. 5 (2014) 4948.
[41] Q.-C. Sun, Y. Ding, S.M. Goodman, H.H. Funke, P. Nagpal, Copper plasmonics and catalysis: role of electron–phonon interactions in dephasing localized surface plasmons, Nanoscale 6 (2014) 12450–12457.
[42] A. Marimuthu, J. Zhang, S. Linic, Tuning selectivity in propylene epoxidation by plasmon mediated photo-switching of Cu oxidation state, Science 339 (2013) 1590–1593.
[43] H.-C. Chu, Y.-C. Chang, Y. Lin, S.-H. Chang, W.-C. Chang, G.-A. Li, H.-Y. Tuan, Spray-deposited large-area copper nanowire transparent conductive electrodes and their uses for touch screen applications, ACS Appl. Mater. Interfaces 8 (2016) 13009–13017.
[44] H.-J. Yang, S.-Y. He, H.-Y. Tuan, Self-seeded growth of five-fold twinned copper nanowires: mechanistic study, characterization, and SERS applications, Langmuir 30 (2014) 602–610.
[45] V.C. Holmberg, T.D. Bogart, A.M. Chockla, C.M. Hessel, B.A. Korgel, Optical properties of silicon and germanium nanowire fabric, J. Phys. Chem. C 116 (2012) 22486–22491.
[46] H. Wang, F. Tam, N.K. Grady, N.J. Halas, Cu nanoshells: effects of interband transitions on the nanoparticle plasmon resonance, J. Phys. Chem. B 109 (2005) 18218–18222.
[47] U. Hohenester, A. Trügler, MNPBEM – A Matlab toolbox for the simulation of plasmonic nanoparticles, Comput. Phys. Commun. 183 (2012) 370–381.
[48] N.J. Halas, S. Lal, W.-S. Chang, S. Link, P. Nordlander, Plasmons in strongly coupled metallic nanostructures, Chem. Rev. 111 (2011) 3913–3961.
[49] E. Prodan, C. Radloff, N.J. Halas, P. Nordlander, A hybridization model for the plasmon response of complex nanostructures, Science 302 (2003) 419–422.
[50] L.S. Slaughter, Y. Wu, B.A. Willingham, P. Nordlander, S. Link, Effects of symmetry breaking and conductive contact on the plasmon coupling in gold nanorod dimers, ACS Nano 4 (2010) 4657–4666.
[51] W. Rechberger, A. Hohenau, A. Leitner, J.R. Krenn, B. Lamprecht, F.R. Aussenegg, Optical properties of two interacting gold nanoparticles, Opt. Commun. 220 (2003) 137–141.
[52] A.P. Bell, J.A. Fairfield, E.K. McCarthy, S. Mills, J.J. Boland, G. Baffou, D. McCloskey, Quantitative study of the photothermal properties of metallic nanowire networks, ACS Nano 9 (2015) 5551–5558.
[53] M. Yorulmaz, A. Hoggard, H. Zhao, F. Wen, W.-S. Chang, N.J. Halas, P. Nordlander, S. Link, Absorption spectroscopy of an individual fano cluster, Nano Lett. 16 (2016) 6497–6503.
[54] L. Zhou, Y. Tan, D. Ji, B. Zhu, P. Zhang, J. Xu, Q. Gan, Z. Yu, J. Zhu, Self-assembly of highly efficient, broadband plasmonic absorbers for solar steam generation, Sci. Adv. 2 (2016) e1501227.
[55] S. Dai, Q. Li, G. Liu, H. Yang, Y. Yang, D. Zhao, W. Wang, M. Qiu, Laser-induced single point nanowelding of silver nanowires, Appl. Phys. Lett. 108 (2016) 121103.
[56] S.E. Allen, R.R. Walvoord, R. Padilla-Salinas, M.C. Kozlowski, Aerobic copper-catalyzed organic reactions, Chem. Rev. 113 (2013) 6234–6458.
[57] M.B. Gawande, A. Goswami, F.-X. Felpin, T. Asefa, X. Huang, R. Silva, X. Zou, R. Zboril, R.S. Varma, Cu and Cu-based nanoparticles: synthesis and applications in catalysis, Chem. Rev. 116 (2016) 3722–3811.
[58] S. Bhanushali, P. Ghosh, A. Ganesh, W. Cheng, 1D copper nanostructures: progress challenges and opportunities, Small 11 (2015) 1232–1252.
[59] J.E. Hein, V.V. Fokin, Copper-catalyzed azide–alkyne cycloaddition (CuAAC) and beyond: new reactivity of copper(i) acetylides, Chem. Soc. Rev. 39 (2010) 1302–1315.
[60] M. Meldal, C.W. Tornøe, Cu-catalyzed azide − alkyne cycloaddition, Chem. Rev. 108 (2008) 2952–3015.
[61] M. Ahlquist, V.V. Fokin, Enhanced reactivity of dinuclear copper(I) acetylides in dipolar cycloadditions, Organometallics 26 (2007) 4389–4391.
[62] F. Wu, D.-W. Zhang, J. Wang, M. Watkinson, S. Krause, Copper contamination of self-assembled organic monolayer modified silicon surfaces following a “Click” reaction characterized with LAPS and SPIM, Langmuir 33 (2017) 3170–3177.
[63] B.H. Lipshutz, B.R. Taft, Heterogeneous copper-in-charcoal-catalyzed click chemistry, Angew. Chem. Int. Ed. 45 (2006) 8235–8238.
[64] V.V. Rostovtsev, L.G. Green, V.V. Fokin, K.B. Sharpless, A stepwise huisgen cycloaddition process: copper(I)-catalyzed regioselective “Ligation” of azides and terminal alkynes, Angew. Chem. Int. Ed. 41 (2002) 2596–2599.
[65] P. Appukkuttan, W. Dehaen, V.V. Fokin, E. Van der Eycken, A Microwave-assisted click chemistry synthesis of 1,4-disubstituted 1,2,3-triazoles via a copper(I)-catalyzed three-component reaction, Org. Lett. 6 (2004) 4223–4225.
[66] L.D. Pachón, J.H. van Maarseveen, G. Rothenberg, Click chemistry: copper clusters catalyse the cycloaddition of azides with terminal alkynes, Adv. Synth. Catal. 347 (2005) 811–815.